

# Persistent Homology of Delay Embeddings

Saba Emrani, Thanos Gentimis and Hamid Krim

Department of Electrical and Computer Engineering  
North Carolina State University  
Raleigh, NC, USA

March 2013

## Abstract

The objective of this study is to detect and quantify the periodic behavior of the signals using topological methods. We propose to use delay-coordinate embeddings as a tool to measure the periodicity of signals. Moreover, we use persistent homology for analyzing the structure of point clouds of delay-coordinate embeddings. A method for finding the appropriate value of delay is proposed based on the autocorrelation function of the signals. We apply this topological approach to wheeze signals by introducing a model based on their harmonic characteristics. Wheeze detection is performed using the first Betti numbers of a few number of landmarks chosen from embeddings of the signals.

## 1 Introduction

Wheezes are musical abnormal lung sounds, which usually imply obstructive airways diseases, such as asthma and chronic obstructive pulmonary diseases. For patients with chronic illness, continuous and automatic monitoring of the respiratory condition is vital to provide essential information for medical diagnosis. Although auscultation with stethoscopes is an easy and popular way to recognize the musical sound of a wheeze, it is not an ideal tool for continuous monitoring of the respiration condition [1]. Therefore, computer-aided wheeze analysis using sound signal digitization and processing techniques have been developed to reproduce and quantify wheezes [2–4].

Wheezes have different feature used for detection and classification purposes. They are intense, continuous with time duration greater than 150 ms and their frequency range is from less than 100 Hz to more than 1 kHz [3]. The most important characteristic of wheezes signals which is the key component of this study is their harmonic behavior in time domain. The sound waves of the

wheezes in time domain are close to signals with sinusoidal signals with time varying amplitudes and frequencies. Accordingly, we propose a model for wheeze signals based on their harmonic behaviour as a piece-wise sinusoidal function. Next, we show that the wheeze signals are in  $\epsilon$  distance of their corresponding introduced model.

Time-delay coordinate embedding has been mostly used in analysis of dynamical systems [5]. There exists a large body of literature on the application of the delay-coordinate embedding technique to dynamical systems with chaotic attractors [6], [7]. Knudson et al. have used three-dimensional time delay embeddings of human speech signals by approximating the data sets with certain simplicial complexes and analyzing their persistent homology [8]. In this paper, we present an analysis of breathing sound signals including wheeze and non-wheeze sounds based on the concept of persistent homology [9]. The use of persistent homology to recapture the almost harmonic behavior of the wheeze signal is better than other methods since it can detect a persistent hole even when there are small fluctuations in the amplitude of the signal. The autocorrelation function, although its a good first indicator, will be inapplicable if the time segments of the signal were big enough. Persistent homology is in general robust when it comes to noise while the computations involved are relatively fast and use available current software since they basically involve matrix manipulations. This novel approach may lead to a more general theory connecting harmonic-periodic behaviors of vector fields with easy to compute, noise invariant persistent barcodes.

## 2 Modeling

The wheeze signal in time domain resembles that of a sinusoidal wave, justifying their musicality. Accordingly, we propose a model for wheeze signals in time domain as a combination of sinusoidal function with different periods, amplitudes and phases. The proposed model can be represented as

$$w(t) = \sum_{i=1}^n g_i(t) \quad (1)$$

where

$$g_i(t) = \begin{cases} w_i(t) & t_i - 1 \leq t < t_i \\ 0 & \text{otherwise} \end{cases} \quad (2)$$

and  $w_i, i = 1, 2, \dots, n$  are denoted as:

$$w_i(t) = A_i \sin\left(\frac{2\pi}{T_i}t + \phi_i\right), A_i \neq 0. \quad (3)$$

To satisfy the continuity of  $w(t)$ , the phases  $\phi_i$  should conform to the following condition

$$\phi_j = \phi_{j-1} + 2\pi t_{j-1} \left( \frac{1}{T_{j-1}} - \frac{1}{T_j} \right) \quad (4)$$

To evaluate the effectiveness of the proposed model in representing the wheeze signals, we construct a model corresponding to each wheeze signal by generating a signal with same frequency and amplitude as those of the wheeze signal at each time instance. This objective is achieved in two steps; first we estimate the frequency of the signals at different time intervals, then we find the envelope of the signal and multiply it by a sinusoidal function with the frequencies obtained in the first step.

In order to obtain the frequency at each time instance, we find the zero crossing points of wheeze and non-wheeze signal. Next, we define the intervals between successive zero crossing indexes as a random variable denoted by  $d_i, i = 1, 2, \dots, n_z - 1$  where  $n_z$  is the number of zero crossing points of the signal. A monophonic wheeze includes a single frequency or several frequencies initiating and ending at different times. Therefore, the frequency of monophonic wheeze signal is approximately a piece-wise constant function of time. Consequently, we can use the distribution of the random variable  $d_i$  to estimate the frequency of the signal. The deviation of  $d_i$  from its mean value is smaller for wheeze signals than for non-wheeze signals. We can find the time intervals at which the frequency is constant using the distribution of  $d_i$  and detect the intervals with almost constant frequencies denoted by  $T_j, j = 1, 2, \dots, n_f$  where  $n_f$  is the number of different frequencies of the signal. Next, we find the frequency during each time interval as

$$f_j = \frac{1}{2\mu_j} \quad (5)$$

where  $\mu_j, j = 1, 2, \dots, n_f$  denotes the mean value of  $d_i$  during  $T_j$ .

The envelop of the signal can be estimated using critical points of the sound signal in time domain. A point  $(t_0, x(t_0))$  is called a critical point of  $x(t)$  if  $t_0$  is in the domain of  $x(t)$  and either  $x'(t_0) = 0$  or it does not exist. We find all critical points of the recorded sound signal  $x(t)$  with positive amplitude since there is a one to one correspondence between critical points with positive and negative amplitudes, and the absolute values of the amplitudes of each pair including one positive critical point and its corresponding negative one are almost the same with a very high accuracy. Next, we perform an interpolation between positive critical points with appropriate factor to obtain the envelope of the signal denoted by  $a(t)$ . Finally, in order to construct the proposed model and compare it with the real recorded sound signal we multiply the envelop of the signal by

$$u(t) = \sum_{j=1}^n h_j(t) \quad (6)$$

$$h_j(t) = \begin{cases} u_j(t) & t_{j-1} \leq t < t_j \\ 0 & \text{otherwise} \end{cases} \quad (7)$$

where  $t_{j-1}$  and  $t_j$  are the start and end time of interval  $T_j$ , i.e.  $t_{j-1} \leq T_j < t_j$ , and

$$u_j(t) = \sin(2\pi f_j t). \quad (8)$$

Therefore, the constructed model of the signal can be expressed as:

$$v(t) = a(t).u(t) \quad (9)$$

Then, we calculate the distance of the constructed model signal from the actual signal.

**Definition 1.** (*Hausdorff distance*). Let  $(Z, d)$  be a compact metric space and  $A = \{a_1, \dots, a_p\}, B = \{b_1, \dots, b_q\}$  two closed subsets of  $Z$ . The Hausdorff distance between  $A$  and  $B$  is defined as

$$d_{\mathcal{H}}^Z := \max \left( \sup_{a \in A} \inf_{b \in B} d(a, b), \sup_{b \in B} \inf_{a \in A} d(a, b) \right). \quad (10)$$

where  $d(a, b)$  is some underlying norm on the points of  $A$  and  $B$ . In this application we use the  $L_2$  or Euclidean norm.

An equivalent definition is based on  $\epsilon$  neighborhood of subsets as follows

$$d_{\mathcal{H}}^Z := \inf (\epsilon \geq 0 : A \subseteq B_\epsilon, B \subseteq A_\epsilon). \quad (11)$$

where

$$A_\epsilon := \bigcup_{a \in A} \{z \in Z : d(z, a) \leq \epsilon\} \quad (12)$$

which is the set of all points within  $\epsilon$  distance of the set  $A$  or the ball of radius  $\epsilon$  around  $A$ .

Next, we show that for each wheeze signal denoted by  $s(t)$  there exists a function  $w(t)$  as defined in equation (1) such that

$$d_{\mathcal{H}}^Z(s(t), w(t)) < \epsilon \quad (13)$$

and this function is  $v(t)$  as denoted in (9) which is the same as  $w(t)$  constructed using the estimated frequencies and envelop of the recorded sound signals. On the other hand, for non-wheeze signals the Hausdorff distance of the constructed model and the signal is very high which means that the proposed model does not represent non-wheeze signals. As it is clear from Figure 1, the Hausdorff distance of wheeze signal from the model is much less than that of non-wheeze signal. More simulations show that this is in general true for all wheeze and non-wheeze signals validating the proposed model for representing wheeze signals. Thus, the use of this model in the analysis techniques can address the problem of differentiating between wheeze and non-wheeze sound signals quite well.

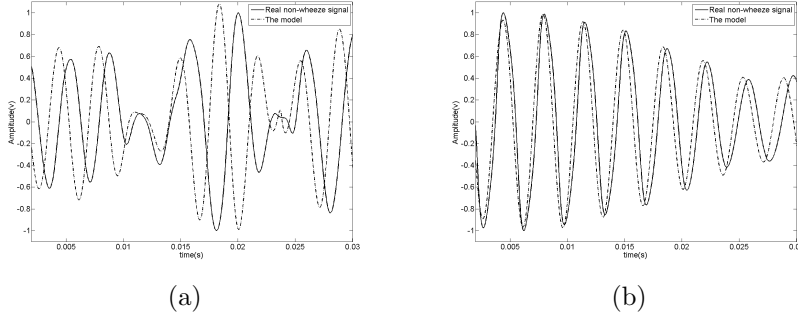


Figure 1: Comparison of the proposed model for (a) a non-wheeze breathing sound signal (b) a wheeze signal

### 3 Time Delay Embeddings

The mathematical foundation of delay-coordinate embedding method was proposed by Packard et al. [10] and Takens [5] to embed a scalar time series into an  $m$ -dimensional space. For each time series  $\{x_i\}, i = 1, 2, \dots$ , the following vector quantity of  $m$  components is constructed:

$$X(t) = (x(t), x(t + \tau), x(t + 2\tau), \dots, x(t + (m - 1)\tau)) \quad (14)$$

where  $x(t) \in \mathbb{R}$ ,  $\tau$  is the delay time and  $m$  is the embedding dimension. A more general representation of delay coordinate embedding can be described as follows:

$$X(t) = (x(t), x(t + \tau_1), x(t + \tau_2), \dots, x(t + \tau_{m-1})) \quad (15)$$

where  $\tau_1, \dots, \tau_m$  are different index delays. In this method, the delay time  $\tau$  and the embedding dimension  $m$  are the two essential parameters. In this study we choose  $m = 2$  and will extend our results to higher dimensional spaces in future works. The 2-dimensional delay-coordinate embedding of time series  $\{x_i\}$  can be expressed as

$$X(t) = (x(t), x(t + \tau)) \quad (16)$$

Discrete time sound signals can be considered as series expressing the amplitude of the wave in volts at each time instance. Thus, we propose using the delay-coordinate embedding approach for analyzing digital signals and extracting their periodic behavior.

#### 3.1 Selecting Time Delay

In order for the delay-coordinate components  $x(t + i\tau), i = 1, 2, \dots, m - 1$  to be independent of each other, the delay time  $\tau$  needs to be chosen carefully. Roughly, if  $\tau$  is too small, then the neighboring coordinate components are too

correlated to be considered as independent coordinates. On the other hand, if  $\tau$  is too large, then adjacent components will be too uncorrelated to this end.

We propose examination of the autocorrelation function of  $x(t)$  to choose a proper delay time. The autocorrelation function finds the correlation of a signal against different time delayed versions of itself. The output of the autocorrelation is the correlation amount as a function of delay time. Clearly, the maximum value will always occur at a delay of zero, since the signal is completely correlated with an exact copy of itself. Other peaks in the autocorrelation function mark delay times at which the signal is comparatively highly correlated with itself. The non-normalized autocorrelation function of the signal  $x(t)$  is calculated as follows

$$R_{xx}(t) = \sum_k x(k+t)x(k) \quad (17)$$

We can also normalize the autocorrelation sequence such that its value at zero delay is 1.

The autocorrelation function of a wheeze and a non-wheeze signal are shown in Figure 2. Clearly, the normalized autocorrelation of a sinusoidal signal is a sinusoidal function with unit amplitude and the same period as the original signal. For the non-wheeze signal, the peaks are relatively short and there does not seem to be any periodic behavior in the autocorrelation. On the other hand, the autocorrelation of wheeze signal changes gradually showing almost periodic behavior. Moreover, it shows peaks with amplitude close to 1 corresponding to the time delays at which the delayed version of the signal is highly correlated to itself.

According to experimental results, the appropriate interval for choosing delay time in order to obtain informative delay embedding of signal  $x(t)$  can be expressed as

$$t_{c1} < \tau < t_{c2} \quad (18)$$

where  $t_{c1}$  and  $t_{c2}$  are the first and second critical points of the autocorrelation function  $R_{xx}(t)$ .

### 3.2 Topology of Delay Embeddings

**Theorem 1.** *The delay-coordinate embedding of  $u(t) = A \sin(\frac{2\pi}{T_1}t)$  using delay  $\tau_1$  can be expressed as*

$$U(t) = \left( A \sin\left(\frac{2\pi}{T_1}t\right), A \sin\left(\frac{2\pi}{T_1}(t + \tau_1)\right) \right) \quad (19)$$

Now, if we change the delay from  $\tau_1$  to  $\tau_2$ , the new delay embedding can be represented as

$$U_1(t) = \left( A \sin\left(\frac{2\pi}{T_1}t\right), A \sin\left(\frac{2\pi}{T_1}(t + \tau_2)\right) \right) \quad (20)$$

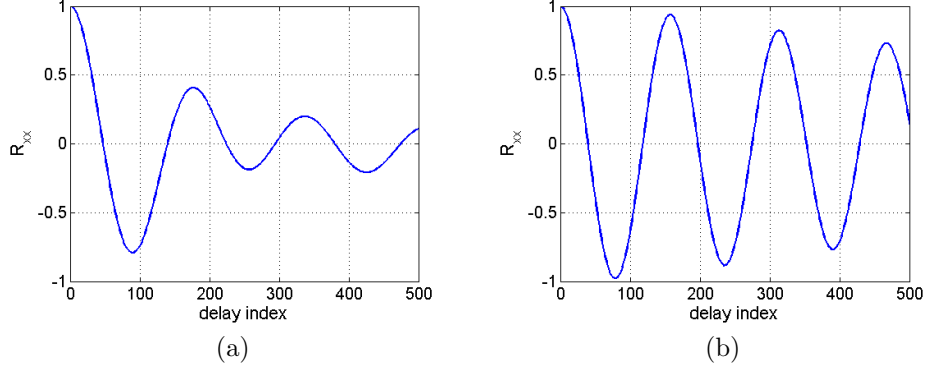


Figure 2: The autocorrelation of (a) a non-wheeze breathing sound signal (b) a wheeze signal

On the other hand, if we use delay  $\tau_1$  and change the period of  $u(t)$  from  $T_1$  to  $T_2$ , the delay-coordinate embedding is going to be

$$U_2(t) = \left( A \sin\left(\frac{2\pi}{T_2}t\right), A \sin\left(\frac{2\pi}{T_2}(t + \tau_1)\right) \right) \quad (21)$$

The delay-coordinate embeddings  $U_1(t)$  and  $U_2(t)$  are equivalent if and only if

$$\frac{\tau_2}{\tau_1} = \frac{T_1}{T_2} \quad (22)$$

*Proof.* Using a change of variable  $t' = \frac{T_1}{T_2}t$ ,

$$\begin{aligned} U_2(t') &= \left( A \sin\left(\frac{2\pi}{T_1}t'\right), A \sin\left(\frac{2\pi}{T_1}t' + \frac{2\pi}{T_2}\tau_1\right) \right) \\ &= \left( A \sin\left(\frac{2\pi}{T_1}t'\right), A \sin\left(\frac{2\pi}{T_1}\left(t' + \frac{T_1}{T_2}\tau_1\right)\right) \right) \end{aligned} \quad (23)$$

So,  $U_1$  and  $U_2$  are equivalent for  $\tau_2 = \frac{T_1}{T_2}\tau_1$ .  $\square$

**Theorem 2.** The delay-coordinate embedding  $W_i(t)$  of  $w_i(t)$  for a fixed  $i$  constructs an ellipse centered at the origin with the angle of rotation  $45^\circ$  provided that  $\tau \neq k\frac{T_i}{2}$  where  $k \in \mathbb{Z}$ . Moreover, the radii of the ellipse can be expressed in terms of the period of the function  $T_i$  and the delay  $\tau$  as

$$\alpha_i = A_i \sqrt{1 - \cos\left(\frac{2\pi}{T_i}\tau\right)}, \quad (24)$$

$$\beta_i = A_i \sqrt{1 + \cos\left(\frac{2\pi}{T_i}\tau\right)}. \quad (25)$$

Therefore, the length of the sides of the circumscribed square around that ellipse equal  $2\sqrt{2}A_i$ .

*Proof.* First we assume that  $A_i = 1$  for simplicity, then generalize the proof for any constant value of  $A_i$ . The trigonometric parametrization of the ellipse can be used for proof. The general quadratic equation  $ax^2 + bxy + cy^2 - \rho = 0$  represents an ellipse with center at origin if the following condition are satisfied:

- 1)  $b^2 - 4ac < 0$ ,
- 2)  $\delta = \begin{vmatrix} 2a & b & 0 \\ b & 2a & 0 \\ 0 & 0 & -2\rho \end{vmatrix} \neq 0$ ,
- 3)  $\delta$  and  $\sigma = a + c$  are of opposite signs.

Moreover, the angle of rotation of the ellipse can be obtained using the following equation

$$\tan(2\theta) = \frac{b}{a - c}. \quad (26)$$

For notion simplification, we assume that  $C := \cos\theta, S := \sin\theta$ . Accordingly, the radii of the ellipse are given as

$$\alpha = \sqrt{\frac{\rho}{P}}, \beta = \sqrt{\frac{\rho}{Q}} \quad (27)$$

where  $P = aC^2 + cS^2 + bCS$  and  $Q = aS^2 + cC^2 - bCS$ . According to Theorem 1, the delay coordinate embedding of  $A\sin(\frac{2\pi}{T}t)$  with delay  $\tau$ , is equivalent to the delay embedding of  $A\sin(t)$  with delay  $\frac{2\pi}{T}\tau$ . Therefore, if we prove that the delay-coordinate embedding of  $\sin(t)$  constructs an ellipse centered at the origin with the angle of rotation  $45^\circ$  provided that  $\tau \neq k\pi$  where  $k \in \mathbb{Z}$ , the first part of the theorem will be proved. Let us construct the quadratic equation using  $x(t) = \sin(t)$  and its delayed version  $y(t) = \sin(t + \tau)$ . Simplifying the obtained equation yields:

$$\sin^2 t(a + b\cos\tau + c\cos^2\tau) + \cos t \sin t(b\sin\tau + 2c\sin\tau\cos\tau) + \cos^2 t(c\sin^2\tau) - \rho = 0 \quad (28)$$

In order for this equation to be true for all times  $t$ , the following conditions should be satisfied

$$\begin{cases} a + b\cos\tau + c\cos^2\tau = c\sin^2\tau \\ b\sin\tau + 2c\sin\tau\cos\tau = 0 \end{cases} \quad (29)$$

Simplifying Equation (29) yields in:

$$\begin{cases} a = c \\ b + 2c\cos\tau = 0 \end{cases} \quad (30)$$

In this case, Equation (28) becomes

$$c\sin^2\tau - \rho = 0 \quad (31)$$

Thus we can check the conditions. First, we can calculate

$$b^2 - 4ac = (-2c\cos\tau)^2 - 4c^2 = 4c^2(\cos^2\tau - 1) \quad (32)$$



Therefore, first conditions is satisfied since  $\tau \neq k\pi, k \in \mathbb{Z}$ . According to Equations (30) and (31), one can calculate  $\delta$  as

$$\delta = -2\rho(4a^2 - b^2) = -8\rho a^2(1 - \cos^2\tau) = -8a^3(1 - \cos^2\tau)^2 \quad (33)$$

which can never be zero since  $\tau \neq k\pi, k \in \mathbb{Z}$ . Moreover, it is of the opposite sign of  $a$  and thus of opposite sign of  $\sigma$ , since  $\sigma = 2a$ . Hence, all three conditions are satisfied and the delay coordinate embedding of  $\sin(t)$  with delay  $\tau \neq k\pi, k \in \mathbb{Z}$  constructs an ellipse centered at the origin. Additionally, according to Equation (26), the angle of rotation is  $45^\circ$ . Also, the same results are true with delay  $\frac{2\pi}{T}\tau$ , where  $\tau \neq \frac{kT}{2}$ . Therefore,  $C = S = \frac{\sqrt{2}}{2}$ . Now, the radii of the ellipse can be calculated. Since

$$\begin{aligned} P &= \frac{a+b+c}{2} = a(1 - \cos\tau) \\ Q &= \frac{a-b+c}{2} = a(1 + \cos\tau), \end{aligned} \quad (34)$$

$\alpha = \sqrt{1 + \cos\tau}$  and  $\beta = \sqrt{1 - \cos\tau}$ . Clearly,  $\alpha, \beta \neq 0$  since  $\tau \neq k\pi$ . So if we change the delay to  $\frac{2\pi}{T}\tau$ , the radii of the ellipse are going to be  $\alpha = \sqrt{1 + \cos(\frac{2\pi}{T}\tau)}$  and  $\beta = \sqrt{1 - \cos(\frac{2\pi}{T}\tau)}$ . Multiplying the amplitude does not change the conditions since it just affects  $\rho$  and multiplies it by  $A^2$  in Equation (28). Therefore the radii of the ellipse would be multiplied by  $A$  according to Equation(27). Since the delay coordinate embedding of  $A\sin(\frac{2\pi}{T}t)$  with delay  $\tau$ , is equivalent to the delay embedding of  $A\sin(t)$  with delay  $\frac{2\pi}{T}\tau$ , the theorem is proved.  $\square$

**Theorem 3.** *Let  $W(t)$  and  $W_i(t)$  be the delay-coordinate embedding of the functions  $w(t)$  and  $w_i(t)$  defined in (1) and (3), respectively. Clearly:*

$$W(t) = \bigcup_{i=1}^n W_i(t) \bigcup K \quad (35)$$

where  $K$  is a finite set of points whose coordinate come from different  $W_i$ 's. In fact, these points are created by neighboring  $W_i$ 's and therefore close to the  $W_i(t)$  or their neighboring embeddings  $W_{i-1}(t)$  and  $W_{i+1}(t)$ .

The proof is straightforward using Equations (1)-(3) and definition of delay embeddings.

**Lemma 1.** *The delay-coordinate embedding  $W_i(t)$  is independent of the phase  $\phi_i$  of  $w_i(t)$ .*

*Proof.* Assume that we have two signals with different phases such as

$$\begin{aligned} w_1(t) &= A \sin\left(\frac{2\pi}{T}t + \phi_1\right) \\ w_2(t) &= A \sin\left(\frac{2\pi}{T}t + \phi_2\right) \end{aligned} \quad (36)$$

So the corresponding delay embeddings are

$$\begin{aligned} W_1(t) &= \left( A \sin\left(\frac{2\pi}{T}t + \phi_1\right), A \sin\left(\frac{2\pi}{T}(t + \tau) + \phi_1\right) \right) \\ W_2(t) &= \left( A \sin\left(\frac{2\pi}{T}t + \phi_2\right), A \sin\left(\frac{2\pi}{T}(t + \tau) + \phi_2\right) \right) \end{aligned} \quad (37)$$

$W_2(t) = W_1(t')$  when  $t' = t + \frac{(\phi_2 - \phi_1)}{2\pi}T$ . Since delay embedding  $W(t)$  is representation of  $w(t + \tau)$  with respect to  $w(t)$  as parameter  $t$  varies,  $W(t) = W(t + c)$  for any constant  $c$ . Accordingly,  $W_1(t) = W_2(t)$ . Thus delay embedding  $W_i(t)$  is independent of phase.  $\square$

**Theorem 4.** *The delay-coordinate embedding  $W(t)$  of  $w(t)$  constructs a set of concentric ellipses with same angle of rotation  $45^\circ$  with different radii and different side lengths of the circumscribed squares around them.*

In fact, in equation (3), if we fix the period  $T_i = T, \forall i$ , the delay-coordinate embedding  $W(t)$  would be a set of concentric ellipses with same angle of rotation  $45^\circ$  and different side lengths of the circumscribed squares around them. On the other hand, with fixing  $A_i = A$ , the delay-coordinate embedding  $W(t)$  constructs a set of concentric ellipses with same angle of rotation and different radii inscribed in a unique circumscribed square with side length of  $2\sqrt{2}A$ .

**Theorem 5.** *The point cloud of delay-coordinate embedding  $W(t)$  of the function  $w(t)$  described in equation (1) with the time delay selected using (18) always has a hole.*

## 4 Persistent Homology

Consider a set of vertices  $V$ . A simplex of dimension  $d$  is defined as the abstract combinatorial object  $[v_1, v_2, \dots, v_{d+1}]$ . The geometric realization of a  $d$ -dimensional simplex, is the the convex hull generated by the vectors  $\vec{e}_i$   $1 \leq i \leq d + 1$  in  $\mathbb{R}^{d+1}$ . A simplex of dimension 0,1,2,3 is respectively a vertex, edge, triangle, pyramid etc. A finite, abstract, simplicial complex is a union of simplices  $K = \sigma_1, \sigma_2, \dots, \sigma_n$  such that for any two simplices  $\sigma_i, \sigma_j$  we have either  $\sigma_i \cap \sigma_j = \emptyset$  or  $\sigma_i \cap \sigma_j = \sigma_k$ , where  $\sigma_k \in K$ . Given a simplicial complex  $K$ , we define an ordered family of vector spaces as follows. Let  $C_i(K)$  be the abstract vector space created over a field  $\mathbb{F}$  such that each simplex of dimension  $i$  is a basis element. Clearly if the dimension of the complex is  $d$  we have  $d + 1$  vector spaces created, namely  $C_0(K), C_1(K), \dots, C_d(K)$ . Then one can define the so-called boundary maps  $\partial_i : C_n(K) \rightarrow C_{n-1}(K)$  for each basis element (simplex) as:

$$\partial([v_0, v_1, \dots, v_n]) = \sum_{i=0}^n (-1)^i [v_0, v_1, \dots, \widehat{v_i}, \dots, v_n]$$

It is easy to check that  $\partial_i \circ \partial_{i-1} = 0$  for all  $i > 0$ . Those boundary operators can be extended to the whole  $C_i(K)$  by linearity. Thus one can obtain a chain

of vector spaces and linear maps:

$$0 \rightarrow C_d(K) \xrightarrow{\partial_d} C_{d-1}(K) \xrightarrow{\partial_{d-1}} \dots \xrightarrow{\partial_3} C_2(K) \xrightarrow{\partial_2} C_1(K) \xrightarrow{\partial_1} C_0 \rightarrow 0$$

This is called a chain complex [9].

The space  $H_n(K) = \frac{\text{Ker} \partial_n}{\text{Im} \partial_{n+1}}$  is called the  $n$ -th dimensional homology (or  $n$ -th homology for short) of the space  $K$ . The dimension of this space is denoted by  $\beta_n = \dim(H_n(K))$  and its called the  $n$ -th Betti number of the space  $K$ . If we are working over fields (which we do) the betti number completely characterizes the  $n$ -th dimensional homology of a space  $K$ .

The  $n$ -th betti number of a metric space intuitively counts the number of “different”  $n$ -dimensional topological features the space  $K$  has. For example,  $\beta_0$  measures the number of connected components,  $\beta_1$  the number of “loops”,  $\beta_2$  the number of “voids” etc.

Given a discrete finite set of points  $X$  in  $\mathbb{R}^n$  and a finite distance  $r$  one can built the Rips Complex,  $K(X, r)$  which is the flag complex on the proximity graph of  $X$ . For increasing values of  $r$ , one gets a nested sequence of simplicial complexes of  $X$ :

$$K_1 \subseteq K_2 \subseteq \dots \subseteq K_i \subseteq \dots \subseteq K_k$$

Let  $H_n^i = H_n(K_i)$ , from the functorial properties of homology one gets a sequence of the form:

$$H_n^1 \rightarrow H_n^2 \rightarrow \dots H_n^i \rightarrow \dots \rightarrow H_n^k$$

A particular class  $\alpha$  may come into existence in  $H_n(K_i)$  and then it either gets mapped to zero in  $H_n(K_s)$  for some  $s > i$  or to a non zero element in the last homology  $H_n(K_k)$ . This yields a barcode, a collection of interval graphs lying above an axis parameterized by  $r$ . An interval of the form  $[t, s]$  corresponds to a class that appears (is born) in  $H_n^t$  and is mapped to zero (dies) at  $H_n^s$ . Classes that live to  $H_n^k$  are represented by the infinite interval, to indicate that such classes are “real” topological features of  $X$ . The collection of all barcodes (for all  $n$ ) is the Persistent Homology diagram of the filtration corresponding to  $X$  and its denoted by  $Dgm(X)$ .

## 4.1 Landmark Selection

In this study, we start with the point cloud  $X$  and choose a smaller set of points  $L \subset X$  using the landmark selection methods of Carlsson and de Silva [11]. In this paper, they have proved that the persistent barcodes of the landmarks well-approximate the barcodes of the original point cloud  $X$  for a large enough number of landmarks. There are three standard options for the choice of landmarks. The first option is selecting the landmarks at random. The second method is the maxmin procedure at which a point  $l_1$  is chosen at random. Then, if  $l_1, \dots, l_n$  have been selected, let  $l_{n+1} \in X - l_1, \dots, l_n$  be the point which maximizes the function

$$z \rightarrow \min\{d(z, l_1), d(z, l_2), \dots, d(z, l_n)\} \quad (38)$$

The third option is using a density-based strategy. The maxmin procedure yields more evenly-spaced landmarks; however it emphasizes extremal points. It is generally more reliable than a random selection [11], on the other hand it requires higher computational complexity. Density-based strategies can be useful in some situations; see, e.g., [12].

## 5 Stability of Persistence

**Definition 2.** [13] *The degree  $p$  Wasserstein distance between persistent diagrams of  $Dgm(X)$  and  $Dgm(Y)$  is defined as:*

$$W_p(Dgm(X), Dgm(Y)) = \left( \sum_l \inf_{\gamma_l} \sum_x \|x - \gamma_l(x)\|_\infty^p \right)^{\frac{1}{p}} \quad (39)$$

where the first sum is over all dimensions  $l$ , the infimum is over all bijections  $\gamma_l : Dgm_l(X) \rightarrow Dgm_l(Y)$ , and the second sum is over all points  $x$  in  $Dgm_l(X)$ .

**Theorem 6.** [14]: *Let  $X$  and  $Y$  be finite point clouds, then*

$$W_\infty(Dgm(X), Dgm(Y)) \leq d_{\mathcal{H}}(X, Y) \quad (40)$$

**Theorem 7.** *The first Betti number of point cloud of delay-coordinate embedding of a wheeze signal with the time delay selected using (18) is always 1.*

The proof is straightforward using theorems 5 and 7 and equation (13).

## 6 Simulation Results

In this study, we considered nine different recorded breathing sound signals [15]: three normal breathing sounds recorded over different areas of body including apex of the lung, midlung, and other chest wall areas and six different type of wheezes including a high pitched, a fixed monophonic wheeze, a random monophonic wheeze, an expiratory polyphonic wheeze, an expiratory stridor, and an inspiratory stridor. The sampling rate is 4.41 kHz. For each wheeze sound signal we chose a small section at which wheezes are heard. We normalized the data so that the maximum amplitude was 1 and the minimum was -1; denote the amplitude at sample point  $t$  by  $x(t)$ . We took the normalized data as input and created a 2-dimensional time delay-coordinate embedding with delay parameter chosen using the autocorrelation function of the sound signal and equation (18). Each of these points lay in the square  $[-1, 1] \times [-1, 1]$ . (Figure 3)

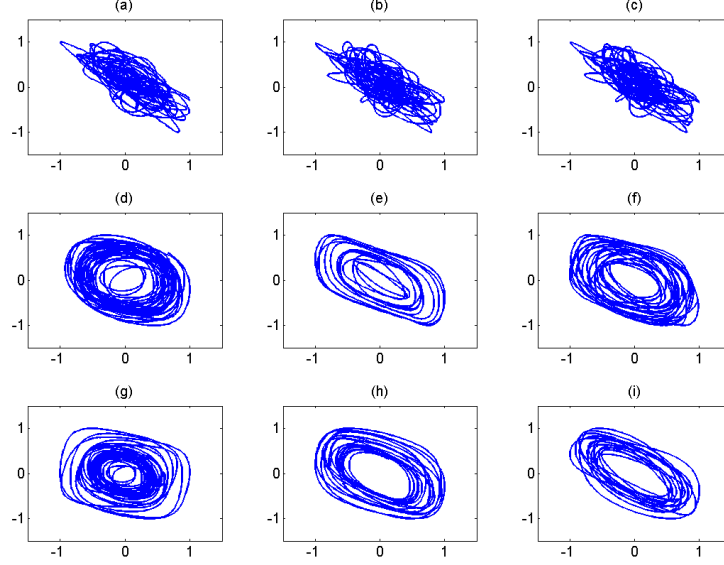


Figure 3: Delay-coordinate embedding of (a) a non-wheeze sound signal recorded over apex, (b) a non-wheeze sound signal recorded over midlung (c) a non-wheeze sound signal recorded over chest wall areas (d) a high pitched wheeze (e) a fixed monophonic wheeze (f) a random monophonic wheeze (g) an expiratory polyphonic wheeze (h) an expiratory stridor (i) an inspiratory stridor

For each point cloud, we constructed a witness complex as follows. We first selected 100 landmarks using maxmin and random procedure described in section 4.1. Figure 4 shows landmarks selected using random and maxmin methods out of delay-coordinate embeddings of a non-wheeze signal recorded over apex and a high pitched wheeze signal. As it is clear in Figure 4, both random and maxmin methods approximate the point cloud quite well in showing the hole inside the delay embedding of the wheeze signal. The random landmark selection technique has two advantages over maxmin method, first it is easier to detect the hole inside landmarks chosen randomly comparing to the ones chosen using maxmin as shown in Figure 4, and second it requires lower computational complexity.

We calculate next the barcodes and Betti numbers  $\beta_0$  and  $\beta_1$  for each sound signal complex.  $\beta_0$  and  $\beta_1$  represent the number of connected components and the number of holes inside the point cloud, respectively. Therefore,  $\beta_0$  is expected to be 1 for the delay embeddings of all signals since they construct one connected component. However,  $\beta_1$  is expected to be 1 for wheeze signals and zero for non-wheeze signals. Accordingly, we can use  $\beta_1$  in order to detect wheezes and distinguish them from normal breathing sounds. Figure 5 demon-

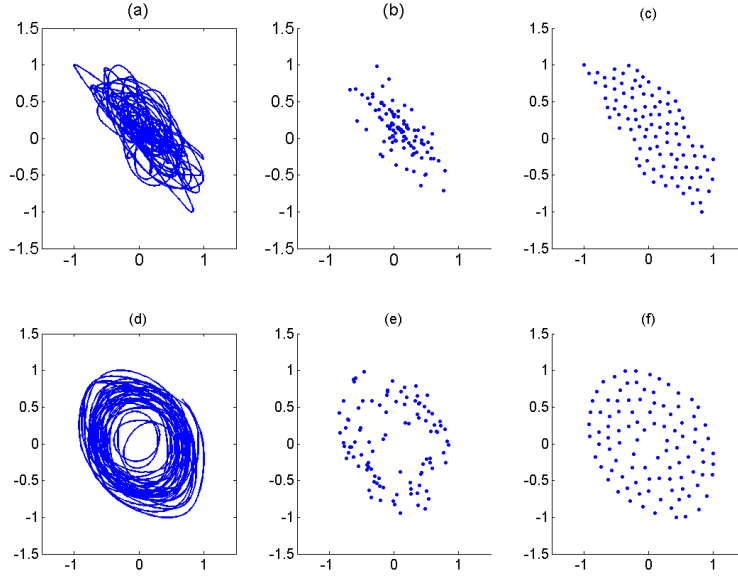


Figure 4: Landmark selection (a)the delay embedding point cloud of a non-wheeze signal including 4000 points, (b) 100 landmarks selected out of (a) using random method, (c) 100 landmarks selected out of (a) using maxmin method, (d) the delay embedding point cloud of a wheeze signal including 4000 points, (e) 100 landmarks selected out of (d) using random method, (f) 100 landmarks selected out of (d) using maxmin method

strates the barcodes for the landmarks of the non-wheeze and wheeze signals shown in Figure (4). More simulation results are included in Figures (6 - 8), where Figures (6) and (7) show the random landmark selections for the point clouds shown in Figure (3), including a fixed monophonic wheeze, a random monophonic wheeze, an expiratory polyphonic wheeze, an expiratory stridor and an inspiratory stridor. Clearly, all point clouds corresponding to wheeze signals have holes. Figure (8) shows the barcodes and Betti numbers for the landmarks represented in Figures (6) and (7). Obviously, the second Betti numbers of the landmarks chosen from delay coordinate embedding for all wheezes are 1 showing the presence of a hole inside their point cloud. We have also performed more experiments using a large number of wheeze and non-wheeze signals that support our statement.

## 7 Conclusion and Future Works

In this work, we introduced a model based on a piece-wise sinusoidal function for wheeze signals according to their harmonic characteristics. The wheeze signals are in  $\epsilon$  Hausdorff distance of the proposed model while the model is not

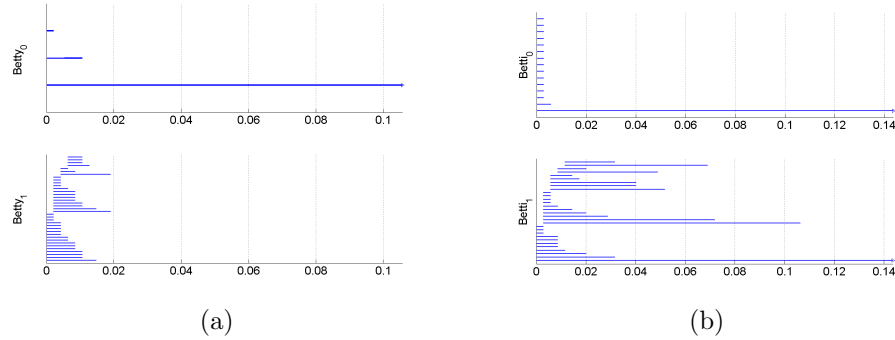


Figure 5: The barcodes for (a) a non-wheeze breathing sound signal (b) a wheeze signal

representative for non-wheeze signal in this sense.

We examined the structure of point clouds generated from delay-coordinate embeddings of breathing sounds in order to detect wheezes and distinguish between normal and wheezing breathing sounds. Delay embedding of a wheeze signal with appropriate value of delay has a hole inside it which is not the case for non-wheeze signals. We have proposed examination of autocorrelation function to select the appropriate delay time to obtain the maximum size hole.

Persistent homology is used as an effective tool for detecting the holes inside the point cloud data. We have selected a few number of landmarks out of so many points representing the sound signal using random and maxmin landmark selection which reduces the computational complexity of the algorithm to a great extent. Random landmark selection outperforms maxmin method due to its lower computational cost and its ability to show the hole inside the point cloud. Our results show that it is possible to detect wheezes according to the second Betti number of their 2-dimensional embeddings. The future work will focus on the structure of the point cloud of higher dimensional delay-coordinate embeddings. Moreover, we will propose a method to detect different frequencies present in an almost periodic signal using the persistent homology of their delay embeddings.

## References

- [1] Y. Shabtai-Musih, J. Grotberg, and N. Gavriely, “Spectral content of forced expiratory wheezes during air, he, and sf6 breathing in normal humans,” vol. 72, pp. 629–35, 1992.
- [2] H. Pasterkamp, S. S. Kraman, and G. R. Wodicka, “Respiratory sounds advances beyond the stethoscope,” vol. 156, pp. 974–987, 1997.
- [3] N. Gavriely, “Breath sounds methodology,” pp. 31–33, 1995.

- [4] G. Charbonneau, E. Ademovic, and B. Cheethan, “Basic techniques for respiratory sound analysis,” vol. 77, pp. 625–635, 2000.
- [5] F. Takens, “Detecting strange attractors in turbulence,” in *Dynamical Systems and Turbulence*, vol. 898 of *Lecture Notes in Mathematics*, pp. 366–381, 1981.
- [6] H. D. I. Abarbanel, R. Brown, J. J. Sidorowich, and L. Sh, “The analysis of observed chaotic data in physical systems,” *Reviews of Modern Physics*, vol. 65, pp. 1331–1392, Oct. 1993.
- [7] H. Kantz and T. Schreiber, *Nonlinear Time Series Analysis*. Cambridge University Press, 1997.
- [8] K. P. Knudson and K. A. Brown, “Nonlinear statistics of human speech data,” vol. 19, pp. 2307–2319, 2009.
- [9] A. Hatcher, *Algebraic topology*. Cambridge: Cambridge University Press, 2002.
- [10] N. H. Packard, J. P. Crutchfield, J. D. Farmer, and R. S. Shaw, “Geometry from a Time Series,” *Physical Review Letters*, vol. 45, no. 9, p. 712, 1980.
- [11] V. De Silva and G. Carlsson, “Topological estimation using witness complexes,” in *Proceedings of the First Eurographics conference on Point-Based Graphics*, pp. 157–166, 2004.
- [12] G. Carlsson, T. Ishkhanov, V. Silva, and A. Zomorodian, “On the local behavior of spaces of natural images,” vol. 76, pp. 1–12, Jan. 2008.
- [13] L. N. Wasserstein, “Markov processes over denumerable products of spaces describing large systems of automata,” *Problems of Information Transmission*, vol. 5, no. 3, pp. 64–72, 1969.
- [14] F. Chazal, D. Cohen-Steiner, L. J. Guibas, F. Mémoli, and S. Y. Oudot, “Gromov-Hausdorff Stable Signatures for Shapes using Persistence,” *Computer Graphics Forum*, vol. 28, no. 5, pp. 1393–1403, 2009.
- [15] Lippincott Williams and Wilkins, *Auscultation Skills: Breath and Heart Sounds*. Princeton University Press, 2009.



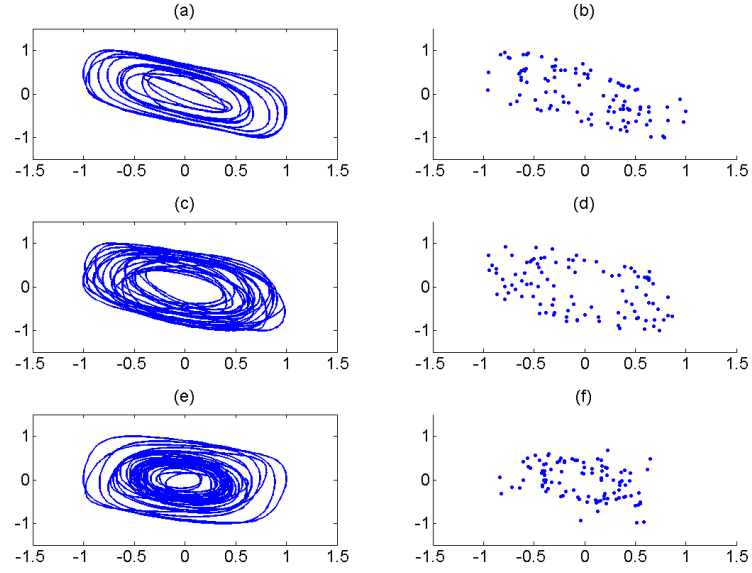


Figure 6: Random landmark selection for different wheezes

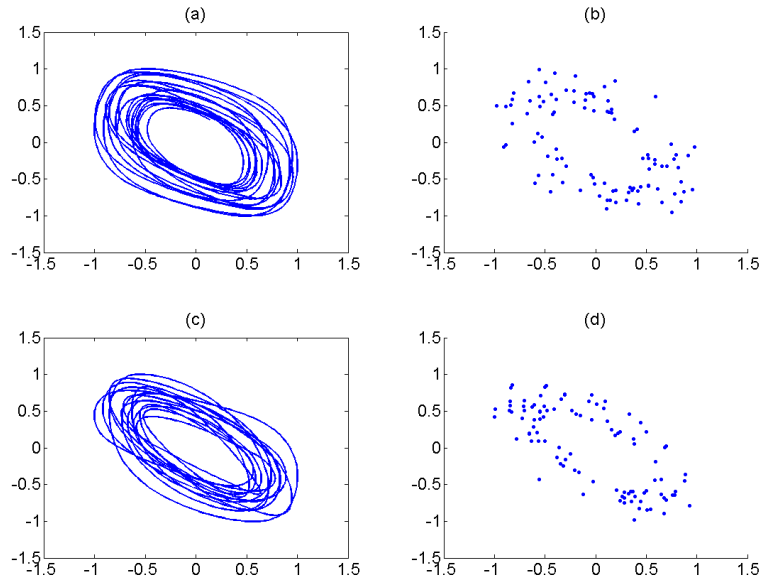
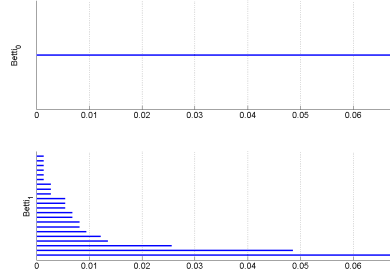
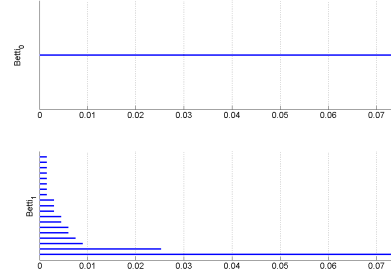


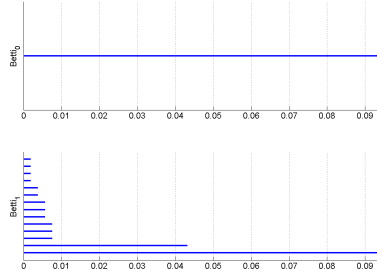
Figure 7: Random landmark selection for different wheezes (stridors)



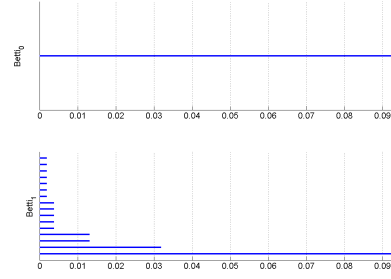
(a)



(b)



(c)



(d)

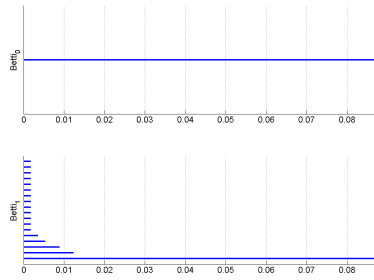


Figure 8: The barcodes for different wheeze signals